A simple dynamical model of the warm-water branch of the mid-depth meridional overturning cell

R. M. Samelson

College of Oceanic and Atmospheric Sciences
104 COAS Admin Bldg
Oregon State University
Corvallis, OR 97331-5503 USA
rsamelson@coas.oregonstate.edu

Submitted to *J. Phys. Oceanogr.*

October 31, 2008

Abstract

A reduced-gravity model is presented of the warm-water branch of the mid-depth meridional overturning circulation in a rectangular basin with a circumpolar connection. The model describes the balance between production of warm water by Ekman advection across the circumpolar current, dissipation of water water by eddy fluxes southward across the current, and the net production or dissipation of warm water by diabatic processes north of the current. The results emphasize the role of the eastern boundary condition in setting the thermocline structure north of the current, and the nonlinear interactions between wind forcing, eddy fluxes, and diabatic mixing, which together control the structure and amplitude of the model meridional overturning circulation. Solutions are shown to exist in which the northward Ekman transport across the circumpolar current is completely compensated by southward eddy fluxes, and the meridional overturning north of the current is entirely driven by diabatic forcing and interior upwelling through the base of the layer. Other solutions are shown to exist in which the interior upwelling into the warm layer at mid-latitudes is negligible, and the meridional overturning circulation consists of a continuous cell that carried the fluid delivered by the northward Ekman transport across the circumpolar current through midlatitudes to the northern hemisphere subpolar gyre, where it cools and returns to depth. The results emphasize that the coupled elements of wind-driving, eddy fluxes, and diabatic processes are inextricably intertwined in the mid-depth meridional overturning circulation.

1 Introduction

The mid-depth cell of the ocean's zonally integrated meridional overturning circulation, consisting loosely of the southward flow of North Atlantic Deep Water from northern subpolar latitudes to the southern hemisphere, and the compensating northward flow of warm thermocline waters from the southern hemisphere to the northern subpolar gyre, is a central element of the large-scale ocean circulation, which likely plays a major role in the Earth's climate system (Schmitz, 1996ab). Lying between the wind-driven (Luyten et al., 1983) upper thermocline gyres above, and the diffusion-driven (Stommel and Arons, 1960; Stommel and Webster, 1962) abyssal circulation below, this cell is evidently driven by a poorly understood combination of these same two mechanisms.

Early theoretical efforts to explore the dynamics of this cell focused on the diffusive mechanism, in which diabatic forcing in the form of interior turbulent mixing drives heat downward, resulting in midlatitude upwelling, and subsequent flow of warm water to the poles, where it cools and sinks (Robinson and Stommel, 1959; Stommel and Webster, 1962). Some observational compendia continue to provide support for this view of the circulation (Munk and Wunsch, 1998; Talley, 2003; see, e.g., discussion in Samelson, 2004).

Recently, numerical model results in simplified geometries, following the pioneering work of Gill and Bryan (1971), have emphasized the importance of the basin geometry in the southern hemisphere, with its circumpolar connection, and have been interpreted to suggest instead that the amplitude of the overturning cell is controlled by southern hemisphere winds (Toggweiler and Samuels, 1995). Related work suggests the importance of eddy fluxes across the circumpolar current in establishing the balances that control the overturning cell (Gnanadesikan, 1999; Hallberg and Gnanadesikan, 2001, 2006; MacCready and Rhines, 2001).

Here, a simple, closed dynamical model of the warm-water branch of the mid-depth meridional overturning cell is constructed and analyzed. This model extends several previous related reduced-gravity models (Veronis, 1978; Samelson, 1999, 2004) by including representations of frictional, eddy, and diabatic processes, such that explicit solutions can be obtained in closed basins. The purpose of this analysis is to develop an accessible dynamical framework in which the dependence of the mid-depth meridional overturning on the balances between southern hemisphere wind forcing, eddy fluxes across the circumpolar current, and diffusive interior diabatic forcing can be efficiently explored and illustrated. This warm-water balance has been previously explored in the scaling and box-model analyses of Gnanadesikan (1999) and Johnson et al. (2007); the analysis also has commonalities with the numerical study by Greatbatch and Lu (2003), but differs in that the latter was based instead on a vertical mode truncation, and did not include a representation of circumpolar-current eddy fluxes. For the present model (Section 2), both numerical (Section 3) and analytical (Section 4) solutions are obtained for the circulation in the warm-water layer and the three components of the warm-water balance; the results illustrate basic dynamical elements of this balance, including the central role of the eastern boundary thermocline depth (Section 5).

2 Model

Let the warm water branch of the meridional overturning circulation be represented (Fig. 1) by a single homogeneous layer of depth h on a β-plane in a rectangular domain $\{x_W < x <$

$x_E, y_S < y < y_N\}$, with depth-integrated zonal and meridional momentum equations given by

$$-fvh = -\gamma h h_x - rhu + \tau^x(x,y), \tag{1}$$

$$fuh = -\gamma h h_y - rhv + \tau^y(x,y). \tag{2}$$

Here $f = \beta y$ is the Coriolis parameter, x and y are zonal and meridional coordinates, u and v are the corresponding horizontal velocities, $\gamma = g\Delta\rho/\rho_0$ is the reduced gravity based on the density difference $\Delta\rho$ between the warm water layer and the fluid beneath, r is a constant friction coefficient that supports a Stommel ($e^{-\beta x/r}$) western boundary layer, and τ^x and τ^y are the zonal and meridional components of the imposed kinematic wind stress. A presumption of the formulation is that the warm water branch of the mid-depth cell lies above the main, internal thermocline and is subject to the direct action of wind, at least in the sense of ventilated thermocline theory (Luyten et al., 1983; Samelson and Vallis, 1997), which here is represented in its most simplistic form by a single active layer.

In the steady-state mass balance, the divergence of horizontal transport in the layer is equal to the upward diabatic velocity W at the base of the layer,

$$(hu)_x + (hv)_y = W(x,y), \tag{3}$$

A positive diabatic velocity, $W > 0$, represents conversion of cold fluid to warm fluid by internal turbulent mixing, and addition of fluid to the warm layer, while a negative diabatic velocity, $W < 0$, represents conversion of warm fluid to cold fluid by surface cooling, and expulsion of fluid from the warm layer (Fig. 1). The diabatic velocity W is taken here to be proportional to the difference of the square of the layer thickness h and an imposed function $h_*^2(x,y)$, which can be chosen to represent heating at midlatitudes and cooling near the poles,

$$W(x,y) = -\alpha_w[h^2(x,y) - h_*^2(x,y)], \tag{4}$$

where α_w is a given constant of proportionality, and h_*^2 is a given function of x and y. Although numerical solutions are possible for general dependencies of W on h and diabatic forcing, this particular choice allows a convenient analytical solution for small α_w, which will be developed below. Note that this formulation is equivalent to the sum of a fixed, spatially varying forcing, or mass source, $F_w = \alpha_w h_*^2(x,y)$ and a nonlinear damping, or mass sink, $D_w = -\alpha_w h^2(x,y)$. Since it is only the departure from local balance at each (x,y) that drives the motion, however, interpretation is simpler for the form (4).

Let $\Psi(x,y)$ and $\Phi(x,y)$ be a stream function and a potential function, respectively, for the horizontal transport, so that

$$hu = -\Psi_y - \Phi_x, \quad hv = \Psi_x - \Phi_y. \tag{5}$$

Then

$$\Phi_{xx} + \Phi_{yy} = -W \tag{6}$$

$$(r\Psi_x)_x + (r\Psi_y)_y + \beta\Psi_x = \tau_x^y - \tau_y^x + J(r,\Phi) + \beta\Phi_y - fW \tag{7}$$

where the natural no-normal-flow conditions imply $\nabla\Phi \cdot \mathbf{n} = 0$ and $\Psi = const$ on the contiguous rigid boundaries.

Suppose that the contiguous boundaries are broken at southern latitudes by a circumpolar channel with periodic boundary conditions at $x = \{x_W, x_E\}$ over the latitude interval $y_1 < y < y_2$ and the depth range $0 < z < -h_s$, where the sill depth h_s is a given constant (Fig. 1). An analytical, zonally symmetric, geostrophic circumpolar current may be introduced in the region $y_1 < y < y_2$, at the southern edge of the warm water layer, following Samelson (1999). The vorticity equation (7) may then be solved separately in two domains, $y_S < y < y_1$ and $y_2 < y < y_N$, with the boundary conditions $\Psi(x,y_2) = 0$ and $\Psi(x,y_1) = \Psi_0$,

where $\Psi = \Psi_0$ also on the contiguous rigid boundary for $y < y_1$. The constant value Ψ_0,

$$\Psi_0 = \frac{\gamma}{y_2 - y_1} h_m^2 \frac{1}{2\beta} \ln \frac{f_2}{f_1}, \tag{8}$$

where $f_j = f(y_j),\ j = \{1,2\}$, is chosen to equal the total transport of a zonally uniform geostrophic circumpolar current,

$$u(y,z) = -\frac{1}{f} \frac{\gamma}{y_2 - y_1}(z + h_m), \quad y_1 < y < y_2, \quad -h_m < z < 0, \tag{9}$$

which corresponds by the thermal wind balance to a density field with vertical isopycnals and constant meridional gradient,

$$\frac{\partial u}{\partial z} = -\frac{g}{f\rho_0} \frac{\partial \rho}{\partial y} = -\frac{g}{f\rho_0} \frac{\Delta\rho}{y_2 - y_1}, \quad y_1 < y < y_2, \quad -h_m < z < 0. \tag{10}$$

Here h_m^2 is the zonal-mean depth of the warm-water layer immediately adjacent to the north side of the circumpolar current,

$$h_m^2 = \frac{1}{x_E - x_W} \int_{x_W}^{x_E} h^2(x, y_2)\, dx; \tag{11}$$

zonal variations in the depth of the current are neglected. Note that the depth, or thickness, h_m of the model circumpolar current is a variable to be obtained as part of the solution; it must be less than the sill depth h_s, so that the current is not blocked by the sill, but otherwise does not depend on h_s.

South of y_2, density increases linearly across the current, as specified by (10). Thus, the isopycnal surfaces just beneath the warm layer will outcrop just south of the northern edge $y = y_2$ of the circumpolar current, and the warm-layer thickness h, which has a finite positive value $h(x, y_2) > 0$ at $y = y_2$, will be zero at all latitudes south of y_2: $h(x, y < y_2) = h(x, y_2^-) = 0$ (Fig. 1). It is natural to set the equivalent thickness function $h_*^2(y)$ for the diabatic forcing also

to zero for $y < y_2$, so that

$$h(x,y) = h_*^2(y) = 0, \quad x_W < x < x_E, \quad y < y_2; \tag{12}$$

the southernmost extent of the warm layer then must remain fixed at $y = y_2$.

The net meridional transport across the circumpolar current into the warm water layer is the sum of the Ekman transport T_{Ek} and the eddy flux T_e. The Ekman transport, which is assumed to be warmed by contact with the atmosphere as it crosses the current northward, is given by

$$T_{Ek} = V_{Ek}(x_E - x_W), \quad V_{Ek} = -\frac{\tau^x(y_2)}{f_2}, \tag{13}$$

where V_{Ek} is the vertically integrated Ekman transport per unit longitude. Although various schemes have been proposed, there is no generally accepted theory for the dependence of the eddy fluxes T_e on the large-scale flow. In the absence of such a theory, a maximally simple prescription is adopted here, in which the eddy transport is taken to be proportional to the zonal mean h_m^2 of the squared depth of the warm-water layer on the north side of the current,

$$T_e = V_e(x_E - x_W), \quad V_e = -\alpha_e h_m^2, \tag{14}$$

Here V_e is the vertically integrated eddy transport per unit longitude, and the depth h_m must be determined as part of the solution. Both T_{Ek} and T_e are assumed to be distributed uniformly along the zonal extent of the current, so that

$$\Phi_y(x,y) = -V_{Ek} - V_e, \quad x_W < x < x_E, \quad y_1 < y < y_2. \tag{15}$$

The problem may then be closed by requiring that the net transport into the warm layer vanish,

$$T_{Ek} + T_e + T_{w2} = 0, \tag{16}$$

where

$$T_{w2} = T_w(y_2), \quad T_w(y) = \int_y^{y_N} \int_{x_W}^{x_E} W\, dx\, dy = \int_{x_W}^{x_E} \Phi_y(x,y)\, dx \tag{17}$$

is the total integrated diabatic flux through the base of the warm layer. The equation (16) gives a condition on the layer thickness $h(x,y)$, since it requires that

$$\int_{x_W}^{x_E} \left(\alpha_w \int_{y_2}^{y_N} h^2(x,y)\, dy + \alpha_e h^2(x,y_2) \right) dx = \alpha_w \int_{y_2}^{y_N} \int_{x_W}^{x_E} h_*^2\, dx\, dy + T_{Ek}, \tag{18}$$

in which the right-hand side depends only on imposed quantities. The function $h^2(x,y)$ must also satisfy the horizontal momentum equations, which may be written in the form

$$\frac{\partial}{\partial x}(h^2) = \frac{2}{\gamma}(\tau^x + r\Phi_x - f\Phi_y + f\Psi_x + r\Psi_y) \tag{19}$$

$$\frac{\partial}{\partial y}(h^2) = \frac{2}{\gamma}(\tau^y + r\Phi_y + f\Phi_x + f\Psi_y - r\Psi_x) \tag{20}$$

The equations (19) and (20) must be solved simultaneously with the vorticity equation (7), the divergence equation (6), and the mass balance condition (18).

Although it is not needed for the solution north of the gap, the circulation south of the gap may be taken to be barotropic and driven by a uniform, compensating vertical velocity W_* into the surface Ekman layer,

$$W = W_* = \frac{1}{(x_E - x_W)(y_1 - y_S)} T_{w2}, \quad y_S \le y < y_1, \tag{21}$$

so that

$$\int_{y_S}^{y_1} \int_{x_W}^{x_E} W_*\, dx\, dy - T_{Ek} - T_e = 0. \tag{22}$$

In the circumpolar current region, $y_1 < y < y_2$, V_{Ek} is assumed constant across the current, so that

$$\tau^x(y) = \frac{f}{f_2} \tau^x(y_2) \quad \text{and} \quad W = 0, \quad y_1 \le y < y_2. \tag{23}$$

Then, since

$$\int_{y_S}^{y_N}\int_{x_W}^{x_E} W\,dx\,dy = \int_{y_S}^{y_1}\int_{x_W}^{x_E} W_*\,dx\,dy + T_{w2}, \tag{24}$$

the condition (18) also guarantees that (6) is solvable for Φ on the full domain. The equations (6), (7), (18), (19), and (20) can be solved numerically by an iterative algorithm. For first guess $h(x,y)$, compute $W(x,y)$ and solve the Poisson equations (6) and (7) numerically for $\Phi(x,y)$ and then $\Psi(x,y)$, using (8) to find one boundary constant for Ψ. Both Ψ and Φ may be obtained separately in the the two subdomains $y_S < y < y_1$ and $y_2 < y < y_N$, for the given $h(x,y)$, and only the solution in the northern subdomain is needed for the iteration. With Φ and Ψ known, for the given $h(x,y)$, integrate (19) and (20) numerically from a given (x_0,y_0) to obtain a new estimate of $h(x,y)$, adjusting $h(x_0,y_0)$ and iterating to ensure that (18) is satisfied, and compute the corresponding new estimate of $W(x,y)$. Then repeat this process *ad inifinitum* to convergence for the (Φ,Ψ,h^2) triplet, terminating the iteration when the correction to $h(x_0,y_0)$ becomes sufficiently small or after a sufficiently large fixed number of iterations.

3 Numerical solutions

3.1 Forcing functions and dimensionless parameters

For the solutions considered here, the imposed wind stress τ is taken to be purely zonal,

$$\tau^x = \begin{cases} \tau_0 \cos\frac{3\pi y}{2}, & y_3 = -\frac{1}{3} < y < y_N = 1 \\ \tau_0 \cos\frac{3\pi y}{2} + \tau_1 \frac{1}{2}\left(1 - \cos\frac{\pi(y-y_3)}{y_2-y_3}\right), & y_2 \le y < y_3 = -\frac{1}{3}, \end{cases} \tag{25}$$

and $\tau^y = 0$, and the squared equivalent thickness function $h_*^2(y)$ for the diabatic forcing north of the circumpolar channel is given by

$$h_*^2(y) = \begin{cases} h_0^2 - \delta h_N^2 y^6, & 0 < y < y_N = 1 \\ h_0^2, & y_2 < y < 0, \\ 0, & y_S < y < y_2. \end{cases} \tag{26}$$

Note that h_*^2 may be negative for sufficiently large δh_N^2 and y; by (4), this guarantees local cooling and diabatic flux out of the warm layer ($W < 0$), since the squared physical layer depth h^2 can never be negative. In (7) for Ψ, (23) is used in $y_1 \le y < y_2$, with, in $y_S \le y < y_1$, the southward extension of (25) plus a linear interpolant between the difference (23) minus (25) at $y = y_1$ and zero at $y = y_S$ (Fig. 1b).

The equations may be made dimensionless using the following dimensional scales: gravitational acceleration $g = 10$ m s^{-2}, density $\rho_0 = 1025$ kg m^{-3}, density difference $\Delta\rho = 10^{-3} \times \rho_0$, depth $H = 1000$ m, length $L = 5 \times 10^6$ m, Coriolis parameter $f_0 = 10^{-4}$ s^{-1} and its meridional gradient $\beta_0 = 2 \times 10^{-11}$ m^{-1} s^{-1}, wind stress $\tau_* = 0.1$ N m^{-2}, horizontal velocity $U = \tau_*/(\rho_0 f_0 H) = 10^{-3}$ m s^{-1}, time $T = L/U = 5 \times 10^9$ s $= 160$ yr, and transport $UHL = 5 \times 10^6$ m^3 s^{-1} $= 5$ Sv. The last of these is the scale for the stream and potential functions.

The resulting dimensionless equations have the same form as the dimensional equations above, with the dimensionless parameters now having the following definitions:

$$\begin{aligned} &\gamma = \frac{\tilde{\gamma} H}{f_0 U L} = \frac{g\Delta\rho H}{\rho_0 f_0 U L} = \frac{g\Delta\rho H^2}{\tau_* L} = 20, \qquad f = \frac{\tilde{f}}{\beta_0 L} = \beta y, \quad \beta = \frac{\tilde{\beta}}{\beta_0} = 1, \\ &\tau_0 = \frac{\tilde{\tau}_0}{\tau_*/\rho_0} : -2 \le \tau_0 \le 0, \qquad \tau_1 = \frac{\tilde{\tau}_1}{\tau_*/\rho_0} : -0.5 \le \tau_1 \le 0.5, \\ &h_0^2 = \frac{\tilde{h}_0^2}{H^2} = 1, \qquad \delta h_N^2 = \frac{\delta \tilde{h}_N^2}{H^2} : 0 \le \delta h_N^2 \le 6, \\ &(\alpha_e, \alpha_w) = (\tilde{\alpha}_e, \tilde{\alpha}_w H) T \ : \ 0 \le (\alpha_e, \alpha_w) \le 5, \qquad r = \frac{\tilde{r}}{f_0} = 0.02. \end{aligned} \tag{27}$$

The dimensional parameters $\{\tilde{\gamma}, \tilde{\beta}, \tilde{\tau}_0, \tilde{\tau}_1, \tilde{h}_0, \delta\tilde{h}_N^2, \tilde{\alpha}_e, \tilde{\alpha}_w, \tilde{r}\}$ are introduced here for clarity, and would replace $\{\gamma, \beta, \tau_0, \tau_1, h_0, \delta h_N^2, \alpha_e, \alpha_w, r\}$ in the dimensional forms of the equations. The dimensionless geometric parameters f and β are standard, while τ_0 and τ_1 measure the strength of the wind forcing. The dimensionless reduced-gravity γ characterizes the strength of the density difference between the warm layer and the deeper fluid, consistent with the thermal wind balance for the given depth and length scales and the wind-forced scaling of the horizontal velocity. The parameters α_e and α_w measure the strength of the eddy and diabatic fluxes per unit longitude, relative to the advective time scale $T = L/U$, while the friction coefficient r is naturally scaled by the Coriolis frequency f_0.

The wind stress coeffficients τ_0 and τ_1 were chosen to represent observed annual and zonal mean zonal wind stress profiles, and the mid-latitude equivalent diabatic forcing depth h_0 was chosen to represent the approximate maximum depth of the subtropical main thermocline. Note that the stress profiles have been adjusted so that there is no Ekman pumping in the circumpolar channel latitudes; this is somewhat artificial but necessary to allow the exact zonal flow solution (9). For the diabatic forcing product $\alpha_w \delta h_N^2 = 4$, the corresponding approximate northern-subpolar-area-integrated vertical transport $\frac{1}{4}\alpha_w \delta h_N^2$ is in dimensional value equal to $UHL = 5$ Sv, a reasonable overturning strength for this single-basin model. Interpreted as timescales for volume renewal, α_e and α_w of order one give values of 100-300 yr, reasonably representative of related crude estimates for the observed mid-depth cell. The limits $\alpha_e \to 0$ and $\alpha_w \to 0$ correspond to asymptotically weak eddy fluxes and weak diabatic forcing, respectively. The value of r for the numerical solutions was motivated by a balance between the computational demand of resolution requirements in the western boundary layer and the desire to approach inviscid dynamics in the interior; for the analytical solutions, the inviscid

limit $r \to 0$ is taken. For the solutions discussed here, the western, eastern, southern and northern domain boundaries are set at $x_W = 0$, $x_E = 1$, $y_S = -1$ and $y_N = 1$, respectively, and the circumpolar channel covers the interval $-0.72 = y_1 < y < y_2 = -0.62$. For numerical solution, the Poisson equations were discretized on a 100×100 grid and solved by successive over-relaxation, with a damped correction to $h(x_0, y_0)$ on the outer iteration.

3.2 Solutions

The choice of parameters $\tau_0 = -1, \tau_1 = 0, \delta h_N^2 = 4, \alpha_w = 2, \alpha_e = 1$, with $h_0^2 = 1, \gamma = 20$, $r = 0.02$ and other values as above, gives a solution that bears a general qualitative resemblance to some characterizations of the observed mid-depth thermocline structure and meridional overturning cell in the North Atlantic (Fig. 2). Note that, with $\delta h_N^2 = 4$, the equivalent squared depth h_*^2 for the diabatic forcing is negative near the northern boundary $y = y_N = 1$, leading to locally intense cooling and flux out of the warm layer. For this solution, the streamfunction Ψ shows the familiar pattern of the Sverdrup-Stommel circulation, with anticyclonic subtropical gyres, cyclonic subpolar gyres, and a strong eastward circumpolar current between the two southern hemisphere gyres (Fig. 2a). The gyres are closed by western boundary currents in frictional layers of width r/β; since the circumpolar current is analytically specified, there are no boundary layers on its sides or at the edges of the gap. The transport of the circumpolar current is several times larger than the transport of the subtropical Sverdrup gyres. The layer thickness h deepens westward in the subtropical gyres, reaching a maximum depth just less than 1 adjacent to the western boundary currents, shallows westward in the northern subpolar gyre, reaching a minimum of less than 0.8 adjacent to the subpolar western boundary current, and decreases southward abruptly to zero at the northern edge of the circumpolar current (Fig.

2b).

The meridional overturning flow is described by the potential function Φ, which shows a meridional gradient from the extreme southern to the extreme northern latitudes that is nearly uniform zonally and relatively independent of latitude, except in the subpolar regions (Fig. 2c). This corresponds to northward flow of warm water that is brought to the surface south of the circumpolar current, warmed by the atmosphere as it crosses the current in the surface Ekman layer, and traverses the midlatitude gyres to the northern subpolar region, where it cools and is expelled from the warm layer into the deeper ocean. This circulation is fundamentally diabatic, since, according to (6) and the associated boundary conditions, it is driven entirely by the interior diabatic velocity W and the cross-isopycnal Ekman flux V_{Ek} at the northern edge of the circumpolar channel. The rotational dynamics do not affect the potential flow, and the overturning described by the potential flow is therefore distributed nearly uniformly across the basin, rather than confined to boundary currents. The total interior flow must still satisfy the Sverdrup balance, so the anticyclonic subtropical gyre flow described by the stream function Ψ is intensified in the northern hemisphere, and weakened in the southern hemisphere, by an amount precisely equal to the interior potential flow. In effect, the rotational dynamics, through the streamfunction, act to concentrate the diabatic meridional overturning flow in the western boundary current.

For these parameters, there is very little diabatic exchange through the base of the warm layer at midlatitudes, relative to the strength of the overturning flow (Fig. 3). Except for a weak upwelling in the subtropical gyres, where the relatively shallow layer depth allows weak upward diabatic motion, all of the upwelling into the surface layer occurs south of the circumpolar channel, and the warm water is produced almost entirely by warming of the

surface boundary layer as the Ekman dynamics carry the surface fluid northward across the circumpolar current (Fig. 3ab). Similarly, all of the downwelling out of the surface layer occurs in the northern part of the northern hemisphere, primarily in the subpolar gyre, where the squared equivalent layer depth h_*^2 for the diabatic forcing becomes first much shallower than the warm-water layer and then negative at the most northern latitudes. Thus, the northward meridional overturning transport of warm water (Fig. 3c) is essentially constant between the northern edge of the channel ($y = y_2 = -0.62$) and the central latitudes of the northern hemisphere subtropical gyre ($y \approx 0.4$). The weak subtropical upwelling is stronger in the eastern than in the western basins, due to the westward, wind-driven deepening associated with the warm-layer Sverdrup balance (Figs. 3b, 2)b.

The model solution describes a balance between the import of warm water by cross-isopycnal Ekman transport at the northern edge of the circumpolar channel, the export of warm water by eddy fluxes southward across the channel, and the net import or export of warm water by the diabatic forcing. For this solution, the Ekman transport across the channel is

$$T_{Ek} = \frac{1}{y_2}\cos\frac{3\pi y_2}{2}(x_E - x_W) \approx 1.58, \tag{28}$$

the eddy transport is

$$T_e = -\alpha_e h_m^2 \approx -0.86, \tag{29}$$

and the net northward transport across the channel is

$$T_{Ek} + T_e = 0.73. \tag{30}$$

Thus the Ekman transport in this solution is more than half-compensated by southward eddy fluxes across the channel, and only 46% of the Ekman transport finds its way into the meridional overturning circulation. Since $T_{w2} = -(T_{Ek} + T_e) = -0.73$, this net northward transport

is also equal to the total integrated downwelling through the base of the warm layer north of the channel. For this solution, there is very little midlatitude diabatic upwelling, so the warm branch of the overturning circulation that is represented in the model consists essentially of the northward flow of the surviving Ekman transport across the midlatitude gyres to the subpolar northern hemisphere, where it cools and sinks.

An essential link in the competition between Ekman transport, eddy fluxes, and diabatic conversion is the eastern boundary value h_E of the thickness of the warm layer, which in the inviscid limit must be constant north of the circumpolar channel. In this solution, $h_E \approx 0.93$. The wind-driving causes local variations in the thickness of the layer, but h_E exerts a dominant control over the large-scale structure. Where h_*^2 is less than h_E^2 in the subpolar gyre, cooling and expulsion of warm fluid from the upper layer occur. If h_E deepens sufficiently, this cooling can occur over the whole basin north of the channel. If h_E is shallower, diabatic upwelling can occur at midlatitudes, where $h_*^2 \approx 1$. As h_E deepens, the expulsion of fluid from the warm layer through eddy fluxes southward across the current also increases. The equilibrium that is reached will depend on the relative efficiencies of the diabatic forcing and the eddy fluxes as they seek to balance the Ekman inflow of warm water into the layer. This picture becomes complicated as h_E shallows and midlatitude upwelling occurs, as a portion of the meridional overturning is then driven by the diabatic forcing.

Solutions obtained by doubling either α_w or α_e, and leaving all other parameters unchanged, illustrate the variations in the overturning circulation that arise from variations of these efficiencies (Fig. 4). For $\alpha_w = 4$ and $\alpha_e = 1$, mid-latitude upwelling increases substantially, so that the maximum northward overturning transport nearly doubles at the northern-hemisphere subpolar-subtropical gyre boundary (Fig. 4c). This has little effect on the solution

in the higher latitudes of the southern hemisphere, so the net northward transport across the channel is only slightly increased. Thus, in this solution, the contributions to the maximum overturning transport are shared roughly equally between mid-latitude upwelling and Ekman transport across the circumpolar channel.

For $\alpha_w = 2$ and $\alpha_e = 2$, the southward eddy transport across the channel is substantially increased, compensating most of the northward Ekman transport. However, the warm layer also shallows significantly, so that the midlatitude diabatic upwelling increases, and the maximum northward overturning transport at the northern-hemisphere subpolar-subtropical gyre boundary is only slightly increased over the original case with $\alpha_w = 2$ and $\alpha_e = 1$ (Fig. 4c). In this case, the northward transport is almost all derived from mid-latitude upwelling, rather than from Ekman transport across the channel as in the original case. This transport downwells in the northern subpolar gyre, effectively resulting in a closed, diabatically-driven meridional overturning cell that is confined north of the circumpolar channel.

4 Asymptotic analysis

4.1 Analytical solution

The general dependence of the solutions on parameters can be efficiently explored through examination of an analytical solution that is accurate when the friction constant r and a parameter proportional to α_w are both small.

As $r \to 0$,

$$\beta \Psi_x = -\tau^x_y + \beta \Phi_y - fW, \tag{31}$$

and

$$\frac{\partial}{\partial x}h^2 = \frac{2f^2}{\beta\gamma}\left[-\frac{\partial}{\partial y}\left(\frac{\tau^x}{f}\right) + \alpha_w(h^2 - h_*^2)\right], \tag{32}$$

so that

$$h^2(x,y) = h_*^2 + \frac{1}{\alpha_w}\frac{\partial}{\partial y}\left(\frac{\tau^x}{f}\right) + \left\{h_E^2 - \left[h_*^2 + \frac{1}{\alpha_w}\frac{\partial}{\partial y}\left(\frac{\tau^x}{f}\right)\right]\right\} e^{-\lambda(x_E - x)}, \tag{33}$$

where $h_E = h(x = x_E, y)$ is the constant (by (2)) eastern boundary depth, τ^x is assumed independent of x, and

$$\lambda = \frac{2f^2}{\beta\gamma}\alpha_w = \frac{2\beta\alpha_w}{\gamma}y^2. \tag{34}$$

Suppose that α_w is small enough that $\lambda(x_E - x_W) << 1$. Then,

$$h^2(x,y) \approx h_E^2 + \frac{2f^2}{\beta\gamma}(x_E - x)\frac{\partial}{\partial y}\left(\frac{\tau^x}{f}\right), \tag{35}$$

and

$$\bar{h}^2(y) = \frac{1}{x_E - x_W}\int_{x_W}^{x_E} h^2(x,y)\,dx \approx h_E^2 + \frac{f^2}{\beta\gamma}(x_E - x_W)\frac{\partial}{\partial y}\left(\frac{\tau^x}{f}\right). \tag{36}$$

Let

$$\bar{D}_0^2(y) = \frac{x_E - x_W}{y_N - y}\int_y^{y_N} \frac{f^2}{\beta\gamma}\frac{\partial}{\partial y}\left(\frac{\tau^x}{f}\right) dy = \frac{x_E - x_W}{y_N - y}\left\{\frac{1}{\gamma}\left[(y\tau^x)|_y^{y_N} - 2\int_y^{y_N}\tau^x\,dy\right]\right\}. \tag{37}$$

Then the northward transport of warm water per unit longitude at latitude y is

$$V(y) = -\int_y^{y_N} W(y')\,dy' \approx \alpha_w(y_N - y)\left[h_E^2 + \bar{D}_0^2(y) - \bar{h}_*^2(y)\right], \tag{38}$$

and

$$T_{w2} = -(x_E - x_W)V(y_2) \approx -\alpha_w(x_E - x_W)(y_N - y_2)[h_E^2 + \bar{D}_0^2(y_2) - \bar{h}_*^2(y_2)]. \tag{39}$$

where

$$\bar{h}_*^2(y) = \frac{1}{y_N - y}\int_y^{y_N} h_*^2(y')\,dy'. \tag{40}$$

Assume also that $\partial(\tau^x/f)/\partial y = 0$ at $y = y_2$. Then $h_m^2 = h_E^2$, and it follows from (16) that

$$h_E^2 \approx \frac{V_{Ek} - \alpha_w(y_N - y_2)\left[\bar{D}_0^2(y_2) - \bar{h}_*^2(y_2)\right]}{\alpha_e + \alpha_w(y_N - y_2)}, \tag{41}$$

$$V_e \approx -\alpha_e h_E^2, \tag{42}$$

$$V(y_2) \approx V_{Ek} - \alpha_e h_E^2. \tag{43}$$

For the particular forms of diabatic and wind stress forcing (26) and (25),

$$\bar{h}_*^2(y) = \begin{cases} h_0^2 - (1-y)^{-1}\frac{1}{7}\delta h_N^2(1-y^7), & 0 < y < y_N = 1 \\ h_0^2 - (1-y)^{-1}\frac{1}{7}\delta h_N^2, & y_2 < y < 0, \end{cases} \tag{44}$$

$$\bar{D}_0^2(y) = \begin{cases} -\frac{1}{\gamma}\frac{x_E - x_W}{1-y}\left\{\tau_0\left[y\cos\frac{3\pi y}{2} + \frac{4}{3\pi}\left(1 + \sin\frac{3\pi y}{2}\right)\right]\right\}, \\ \qquad\qquad y_3 = -\frac{1}{3} < y < y_N = 1 \\ -\frac{1}{\gamma}\frac{x_E - x_W}{1-y}\left\{\tau_0\left[y\cos\frac{3\pi y}{2} + \frac{4}{3\pi}\left(1 + \sin\frac{3\pi y}{2}\right)\right]\right. \\ \qquad \left. + \frac{\tau_1}{\gamma}\left[\frac{y}{2}\left(1 - \cos\frac{\pi(y-y_3)}{y_2-y_3}\right) + (y_3 - y) + \frac{y_2 - y_3}{\pi}\sin\frac{\pi(y-y_3)}{y_2-y_3}\right]\right\}, \\ \qquad\qquad y_2 < y < y_3 = -\frac{1}{3} \end{cases} \tag{45}$$

and,

$$V_{Ek} = -\frac{1}{f_2}\left(\tau_0\cos\frac{3\pi y_2}{2} + \tau_1\right) \tag{46}$$

$$\bar{D}_0^2(y_2) = -\frac{1}{\gamma}\frac{x_E - x_W}{1-y_2}\left\{\tau_0\left[y_2\cos\frac{3\pi y_2}{2} + \frac{4}{3\pi}\left(1 + \sin\frac{3\pi y_2}{2}\right)\right] + \tau_1 y_3\right\}, \tag{47}$$

$$\bar{h}_*^2(y_2) = h_0^2 - (1-y_2)^{-1}\frac{1}{7}\delta h_N^2. \tag{48}$$

These expressions may be substituted into (41) to obtain the explicit analytical solution.

For the scales above, $\lambda \leq 0.1\,\alpha_w$, so the analytical solution should be useful for, roughly, $\alpha_w \leq 3$. Comparisons with numerical solutions show that this is the case, and that the analytical solution can provides useful guidance even for larger values of α_w (Fig. 4).

4.2 Analytical results

4.2.1 Complete eddy compensation

In the numerical solution described above with $\alpha_w = \alpha_e = 2$, the Ekman transport T_{Ek} was mostly compensated by the eddy flux T_e, so that T_{w2} was relatively small (Fig. 4c). From the analytical solution, the relations between parameters can be obtained for which $T_{w2} = V(y_2) = 0$, and there is complete compensation of the Ekman transport by the eddy flux. For variable τ_0 and δh_N^2, for any $\alpha_w > 0$, and with other parameter values as in the numerical solutions above, the eddy coefficient α_e that gives this compensation varies over the range $0 < \alpha_e < 8$, and is approximately proportional to τ_0 for fixed δh_N^2 (Fig. 5). Thus, complete shutdown of the wind-driven component of the overturning can be achieved for parameter values that are not extremely different from those for the solutions discussed above. Note that in the analytical limit of small λ, these values of α_e are independent of α_w.

4.2.2 Dependence on α_e and α_w

Relative to other parameters such as the amplitude of the wind stress forcing, accurate or appropriate values of the eddy flux and diabatic forcing constants α_e and α_w are much more uncertain. Thus, it is natural to consider the general dependence of the solutions on these poorly known parameters. For other parameters as in the solutions above, the eastern boundary depth h_E is not strongly sensitive to variations in α_e and α_w when $\alpha_e + \alpha_w \geq 1$ (Fig. 6). As

both α_e and α_w approach zero, however, h_E approaches infinity. Thus, for sufficiently weak eddy activity and diabatic forcing, the warm water depth will extend to the sill depth of the circumpolar channel, at which point the assumed channel geometry is no longer appropriate.

As might be anticipated, the eddy flux V_e depends strongly on α_e, and only weakly on α_w (Fig. 7). However, as $\alpha_w \to 0$, the dependence of V_e on α_e weakens for larger values of α_e. In this regime, α_e has exceeded the value that shuts down the wind-driven overturning, and the net flow meridional flow $V(y_2)$ across the circumpolar current is southward (Fig. 8). The small values of α_w hinder upwelling of additional warm fluid north of the current, leading to the saturation of V_e as α_e increases.

The net meridional flow $V(y_2)$ across the channel is, perhaps surprisingly, nearly independent of α_w, except for $\alpha_w \leq 1/2$, for which the shutdown of diabatic exchange north of the channel, presumably due to the small α_w, results in approximate compensation for any α_e (Fig. 8). $V(y_2)$ also depends on α_w for $\alpha_e > 4$, but this is an apparently unrealistic regime, in which the net transport across the circumpolar current is strongly southward.

4.2.3 Dependence on τ_1

Variations in the parameter τ_0 affect the wind stress over the entire basin. Variations in τ_1, however, affect only the southern hemisphere winds near the circumpolar gap, and the associated northward Ekman transport. The dependence of the solutions on τ_1 can be examined in order to determine the extent to which the model's meridional overturning circulation is driven by the southern hemisphere westerly winds. For $\tau_0 = 1$ as above, the range $-0.5 < \tau_1 < 0.5$ corresponds to a decrease or increase in the southern hemisphere westerly winds of up to 50%, with positive τ_1 giving stronger westerly (eastward) winds.

The dependence of the net northward transport across the current, $V(y_2)$, on τ_1 is strong for most values of α_e, for fixed $\alpha_w = 2$, weakening slightly for large α_e (Fig. 9). Thus, for this fixed value of α_w, the northward transport across the current is strongly controlled by local winds. For fixed $\alpha_e = 1$, this is true as well for larger values of α_w (Fig. 9). For small values of α_w, however, the dependence of $V(y_2)$ on τ_1 weakens, as the eddy fluxes remove the warm layer fluid more efficiently than the diabatic forcing, resulting in weak, approximately compensated transport across the current.

In contrast, for fixed $\alpha_e = 1$, the eastern boundary depth h_E generally depends only weakly on τ_1 for fixed α_w, though more strongly for small α_w (Fig. 10). This is consistent with the approach to the eddy-compensated state, with large values of h_E, for small α_w. For fixed $\alpha_w = 2$, the dependence of the depth h_E on τ_1 is only weakly dependent on α_e, as the northern hemisphere layer thickness and diabatic flux adjust to match the modified northward transport $V(y_2)$ across the current. The dependence of the eddy flux V_e on τ_1 is relatively strong for large α_e and small α_w, and relatively weak for small α_e and large α_w (Fig. 11). Note that the transport V_e itself depends strongly on α_e for fixed α_w, and on α_w when α_e is fixed and small (Fig. 7).

The meridional transport $V(y)$ north of the circumpolar gap and in the northern hemisphere also has a dependence on τ_1 (Figs. 12,13,14). At the equator ($y = 0$), this dependence is diminished roughly by half from the dependence of $V(y_2)$ on τ_1 (Figs. 9,12). In the central latitudes of the northern hemisphere subtropical gyre, this dependence is reduced by roughly half again (Fig. 13). The sign of the difference between the meridional transport in the central northern subtropical gyre and at the equator depends on τ_1, α_e, and α_w (Fig. 14). Thus, for sufficiently strong southern hemisphere winds, small α_e, or small α_w, the northward transport

may be larger at the equator than in the northern subtropical gyre (Fig. 14), with downwelling at all latitudes north of the circumpolar channel. This may be a physically unrealistic regime, arising from the simplistic prescription (4) for the diabatic mass flux through the base of the layer.

5 Discussion

Although highly idealized, the model illustrates several essential aspects of the dynamics of the mid-depth meridional overturning. Solutions were shown to exist in which the northward Ekman transport across the circumpolar current was completely compensated by southward eddy fluxes, and the meridional overturning north of the current was entirely driven by diabatic forcing and interior upwelling through the base of the layer. Other solutions were shown to exist in which the interior upwelling into the warm layer at mid-latitudes was negligible, and the meridional overturning circulation consisted of a continuous cell that carried the fluid delivered by the northward Ekman transport across the circumpolar current through midlatitudes to the northern hemisphere subpolar gyre, where it cooled and returned to depth. Thus, the distinction between meridional overturning driven by southern hemisphere winds and by interior diapycnal fluxes proves, in this model, to be one of degree: both types of solution are possible, and it is the relative values of critical parameters that determines the regime.

The model also illustrates the critical role of the eastern boundary layer depth h_E in setting the thermocline structure north of the current. Since this depth is communicated instantaneously, in this approximation, along the eastern boundary, it effectively controls the mean difference between the squared layer depth h^2 and the squared equivalent diabatic forcing depth h_*^2 throughout the warm water layer, and thus also the net diabatic flux through the

base of the warm layer. At the southern edge of the warm layer, this same depth controls the strength of the eddy fluxes across the circumpolar current, as well as the zonal transport of the current itself. Thus, it is an essential mediator in the competition between eddy fluxes and interior diabatic fluxes that determines the amplitude of the overturning cell.

Through these dependencies, the model provides an explicit, analytical demonstration of the inextricable intertwining of the coupled elements of wind-driving, eddy fluxes, and diabatic processes in the mid-depth meridional overturning circulation. In general, the three-way balance between these sources and sinks of warm fluid is such that the dependence of the circulation on any variations in any one process depends on the particular regimes in which the others are operating in any given solution. For example, in order to stay on the completely compensated solution, with no net transport across the circumpolar current, while varying the wind stress amplitude τ_0 and holding other parameters constant to the extent possible, it is necessary to alter either α_e or δh_N^2 by precisely the right amount (Fig. 5). On the other hand, some parts of the circulation, in some regimes, can become essentially independent of others. For example, the dependence on southern hemisphere winds of the net meridional transport across the circumpolar current becomes essentially independent of the diabatic forcing efficiency α_w for $\alpha_e = 1$ and $\alpha_w \geq 1$ (Fig. 9).

Dimensional results for the solutions above may be obtained using the scales introduced above in Section 3.1. The dimensional zonally integrated meridional Ekman transport across the circumpolar gap is only 8 Sv, and the maximum meridional overturning transports are only 4-8 Sv (Fig. 4). However, these transports scale with the zonal width of the basin, which here is only 5000 km. Since the solution is periodic in the circumpolar channel, three identical domains can be attached in series to extend the domain zonally, as a crude rep-

resentation of the three major ocean basins. The corresponding zonally integrated Ekman and meridional overturning transports would be 24 Sv and 12-24 Sv, respectively, similar to oceanographic observations of these quantities, although the overturning would be unrealistically shared equally between the three basins. In that sense, the dimensional amplitude of the meridional overturning is broadly consistent with existing observations; however, while the integrated area and volume flux quantities may then be roughly appropriate, the equipartition of overturning between basins in such a zonally replicated model is not. Similarly, the nominal 1000-m midlatitude depth, implied by the model results, of the isopycnal on the northern side of the circumpolar current may be considered in rough accord with large-scale observations of ocean density structure; this is no surprise, since observations motivated the choice of values for the quantities h_0 and H. Since the density difference $\Delta\rho$ between the warm layer and the underlying fluid was also chosen based on oceanographic values, the implied heat transports associated with these volume transports, and the implied mixing rates associated with the diabatic forcing, are also, by construction, broadly consistent with oceanographic estimates.

Various elements of the present model and results have been preceded and anticipated by several related studies. Following Toggweiler and Samuels (1995), McDermott (1996) used coarse-resolution primitive-equation numerical experiments to explore the dependence of meridional overturning transport on southern hemisphere winds, including both the influence of the circumpolar channel and the time-dependent adjustment process, for a similar idealized basin geometry; the results showed a dependence of northern overturning on southern hemisphere winds, but did not address the role of variable diabatic mid-latitude or cross-channel eddy fluxes, nor were any analytical solutions presented. In a more recent numerical study, Greatbatch and Lu (2003) used a reduced-gravity model to explore the role of southern

hemisphere winds in meridional overturning and the dynamical accuracy of parameterizations of overturning in terms of meridional, rather than zonal geostrophic, pressure gradients, and compared their results to the differing abyssal circulation paradigms of Stommel (1961) and Stommel and Arons (1960); they found that box-model, zonal-average balances appeared to represent the overturning dynamics more accurately when southern hemisphere winds were added to the reduced-gravity model.

Of more direct relevance is the scaling argument of Gnanadesikan (1999), which exploited a similar conceptual warm-water balance of Ekman transport, eddy fluxes, and diabatic mid-latitude upwelling to obtain an average oceanic pycnocline depth scale D. Cross-channel eddy fluxes were taken as linearly proportional to D, rather than the quadratic dependence on the local layer-depth parameter h_m (14) assumed here, and the equations were closed by a downstream frictional balance in the western boundary currents, with fixed friction coefficient chosen to match the observed overturning transport, rather than through a thermodynamic balance constraint and direct representation of the northern hemisphere diabatic sinking. Mid-latitude upwelling was taken to be inversely proportional to D, differing from the present formulation (4); this prevented any possibility of the presumably unphysical mid-latitude downwelling, but introduced a singularity as $D \to 0$. It is hard to argue persuasively for the relatively superiority of any of these four crude representations of eddy and diabatic fluxes. On the other hand, both the asymptotic $r \to 0$ solution derived here as well as numerical solutions with variable r of the present model indicate that the assumption of frictional control is both unnecessary and inappropriate for the small values of friction parameters that are arguably, on the basis of boundary-current-width and other simple estimates, representative of the strength of ocean frictional processes. The relatively linear dependencies found by Gnanadesikan (1999)

of D, northern hemisphere sinking, and low-latitude upwelling on the eddy flux, diabatic upwelling, and wind stress parameters, are generally consistent with the results presented here, but the assumed frictional dependence of the overturning in that study obscured the important role of the eastern boundary depth h_E that was exhibited and discussed above.

This role of h_E is anticipated and emphasized in the recent extension of the Gnanadesikan (1999) scaling analysis by Johnson et al. (2007), who interpret the quantity D as an eastern boundary thermocline depth. The scaling, or box-model, equations of Johnson et al. (2007) also include a separate salt balance, following Stommel (1961), and support regimes with multiple equilibria for the overturning circulation. The inclusion of a salt balance seems to be necessary for such multiple equilibria, which are not found in the scaling equations of Gnanadesikan (1999) or the present model. Johnson et al. (2007) include time-dependent effects as well, and find a parameter regime in which oscillations between the two circulation patterns occurs.

6 Summary

The simple model of the warm-water branch of the mid-depth meridional overturning cell considered here provides explicit illustration of central dynamical elements of the overturning circulation. The results emphasize the role of the eastern boundary condition in setting the thermocline structure north of the current, and the nonlinear interactions between wind forcing, eddy fluxes, and diabatic mixing, which together control the structure and amplitude of the model overturning cell. It is hoped that this model will be useful in the formulation, interpretation, and analysis of the more complex and realistic models that must ultimately be used to represent the observed circulation.

A number of natural extensions of this simple model suggest themselves, which may also prove useful to consider. It would be relatively straightforward to recast this model in a time-dependent form, in order to explore the time-dependent response to changes in external forcing or parameters. This could be done by restoring the local time rate of change of the layer thickness in the mass conservation equation (3). The dynamics of the southward return flow in the underlying fluid could be explicitly represented, by including an active deep layer. A more detailed representation of upper thermocline structure in the midlatitudes and tropics could be explored, following Luyten et al. (1983), to replace the present, single, homogenous warm layer.

Acknowledgments

This research was supported by the Division of Ocean Sciences of the National Science Foundation, Grant OCE-0424516.

References

Gill, A., and F. Bryan, 1971. Effects of geometry on the circulation of a three-dimensional southern hemisphere ocean model. *Deep-Sea Res.*, **18**, 685–721.

Gnanadesikan, A., 1999. A simple predictive model for the structure of the oceanic pycnocline. *Science*, **283**, 2077–2079.

Hallberg, R., and A. Gnanadesikan, 2006. The Role of Eddies in Determining the Structure and Response of the Wind-Driven Southern Hemisphere Overturning: Results from the Modeling Eddies in the Southern Ocean (MESO) Project. *J. Phys. Oceanogr.*, **36**, 2232–2252.

Hallberg, R., and A. Gnanadesikan, 2001. An Exploration of the Role of Transient Eddies in Determining the Transport of a Zonally Reentrant Current. *J. Phys. Oceanogr.*, **31**, 3312–3330.

Luyten, J., J. Pedlosky, and H. Stommel, 1983. The ventilated thermocline. *J. Phys. Oceanogr.*, **13**, 292–309.

MacCready P., and P. B. Rhines, 2001. Meridional transport across a zonal channel: Topographic localization. *J. Phys. Oceanogr.*, **31** (6): 1427–1439.

Munk, W., and C. Wunsch, 1998. Abyssal recipes II: energetics of tidal and wind mixing. *Deep-Sea Res. I*, **45**, 1977–2010.

Robinson, A. R., and H. Stommel, 1959. The oceanic thermocline and the associated thermohaline circulation. *Tellus*, **11**, 295–308.

Samelson, R. M., 1999. Geostrophic circulation in a rectangular basin with a circumpolar connection. *Journal of Physical Oceanography*, **29**, 3175-3184.

Samelson, R. M., 2004. Simple mechanistic models of mid-depth meridional overturning. *Journal of Physical Oceanography*, **34**, 2096-2103.

Samelson, R., and G. K. Vallis, 1997. Large-scale circulation with small diapycnal diffusion: the two-thermocline limit. *J. Mar. Res.*, 223-275.

Schmitz, W. J., Jr., 1996ab. On the world ocean circulation: Volumes I and II. Woods Hole Oceanogr. Inst. Tech. Reps., WHOI-96-03, WHOI-96-08.

Stommel, H., 1961. Thermohaline convection with two stable regimes of flow. *Tellus*, **13**, 224–230.

Stommel, H. and A. Arons, 1960. On the abyssal circulation of the world ocean–I. Stationary planetary flow patterns on a sphere. *Deep-Sea Res.*, **6**, 140–154.

Stommel, H. and J. Webster, 1962. Some properties of the thermocline equations in a subtropical gyre. *J. Mar. Res.* **44,** 695–711.

Talley, L., 2003. Shallow, intermediate, and deep overturning components of the global heat budget. *J. Phys. Oceanogr.*, **33**, 530–560.

Toggweiler, R., and B. Samuels, 1995. Effect of Drake Passage on the global thermohaline circulation. *Deep-Sea Res.*, **42**, 477–500.

Veronis, G., 1978. Model of world ocean circulation, III. Thermally and wind-driven. *J. Mar. Res.*, **36**, 1-44.

List of Figures

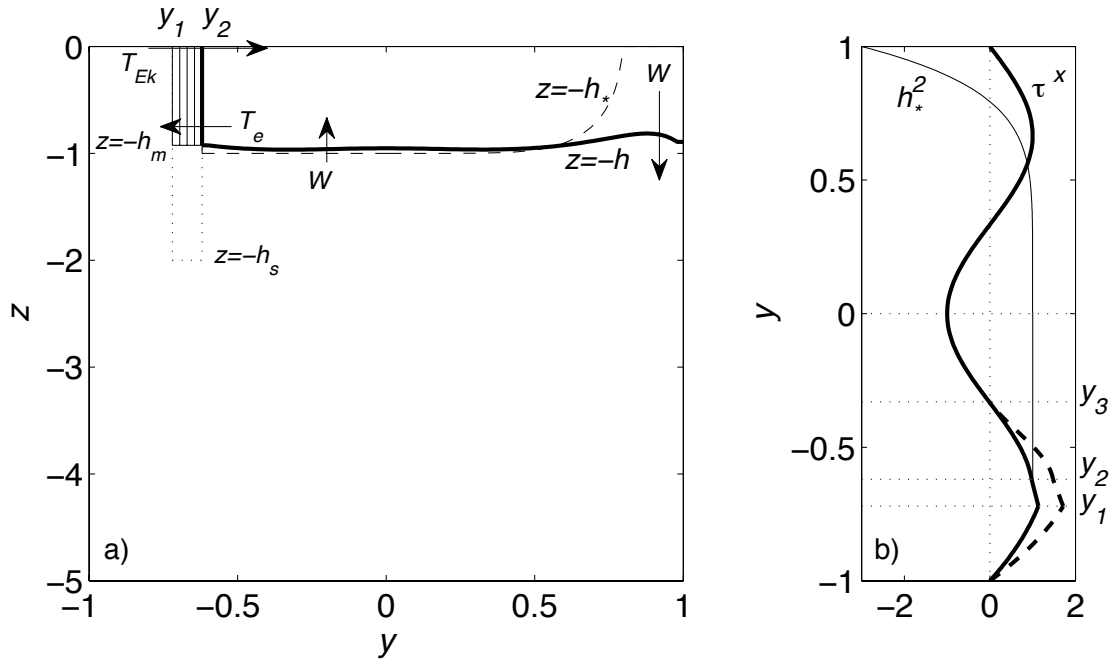

Figure 1: (a) Schematic model-cross-section, showing model warm-layer depth $z = -h$ (thick solid line) and equivalent diabatic forcing depth $z = -h_*$ (dashed line) vs. dimensionless latitude y and depth z. The model circumpolar current flows through a circumpolar gap $y_1 < y < y_2$, $-h_s < z < 0$ (dotted line), at which the eastern and western boundary conditions are periodic, and which extends beneath the current to the sill depth $z = -h_s$. The vertical isopycnals of the model circumpolar current associated with the warm layer (thin solid lines) fill the upper portion of the circumpolar gap to the depth $z = -h_m$, which lies above the sill and is equal to the zonal mean of h at $y = y_2$. There are three types of transport into and out of the warm layer (arrows): the northward near-surface Ekman transport T_{Ek} and southward interior eddy flux T_e across the gap, and the vertical diabatic fluxes $W(x,y)$ across the base of the warm layer; the latter typically include both upwelling at mid-latitudes and downwelling at high northern latitudes. The additional southern hemisphere wind stress proportional to τ_1 is zero for $y > y_3$.

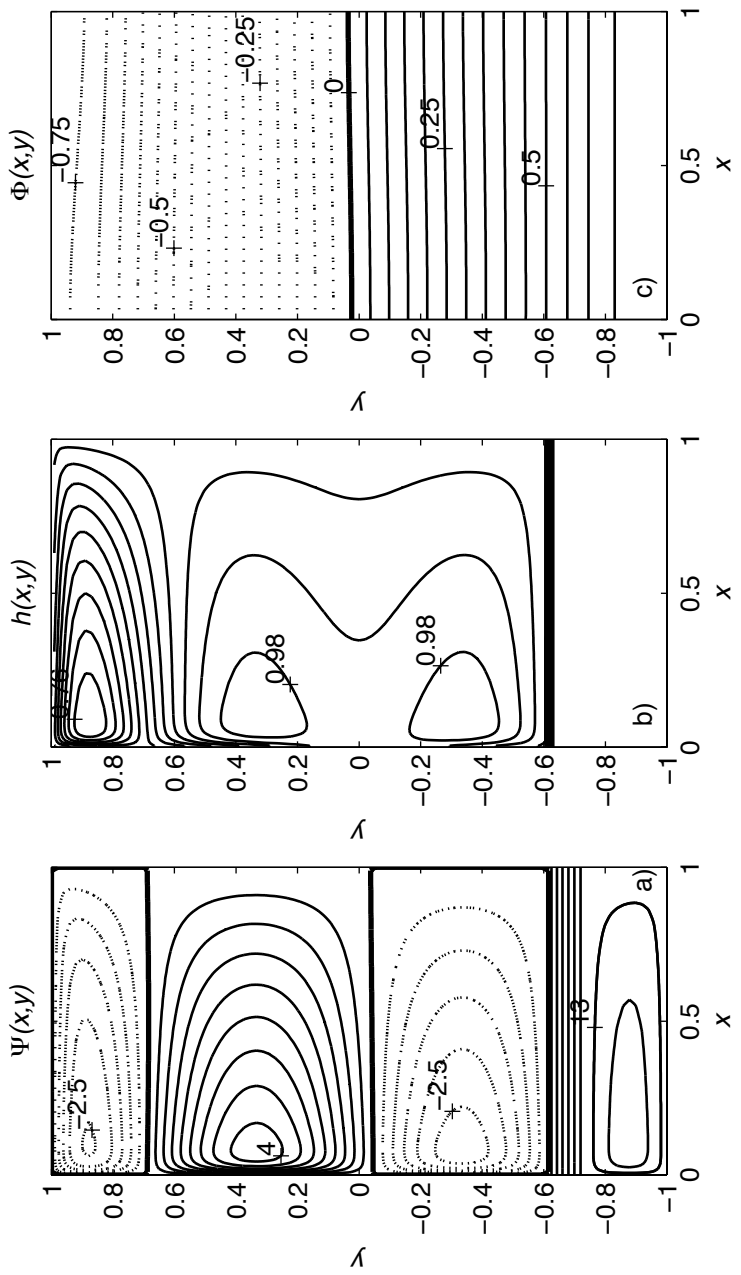

Figure 2: Contours vs. x and y for numerical solution with $(\alpha_w, \alpha_e) = (2,1), \tau_0 = -1, \tau_1 = 0, h_0 = 1, \delta h_N^2 = 4, \gamma = 20, r = 0.02, \beta = 1$: (a) Ψ (contour interval (CI) = 0.5, with CI = 2 in $y_1 = -0.72 < y < y_2 = -0.62$ and CI=1 for $y < y_1$), (b) h (CI = 0.02; $h = 0$ for $y < y_2$), (c) Φ (CI = 0.05).

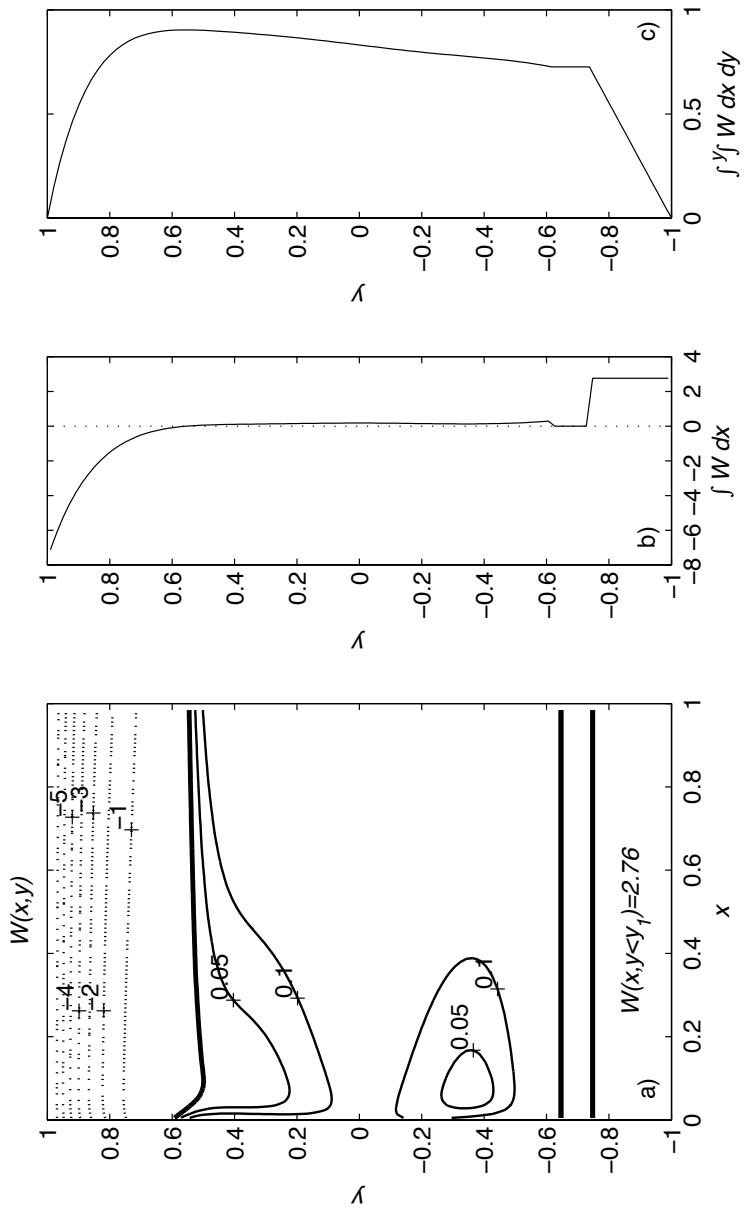

Figure 3: (a) Contours of W vs. x and y (CI = 1 for $W < 0$ and CI = 0.05 for $W > 0$) and zonally integrated (b) vertical velocity $\int_{x_W}^{x_E} W(x,y)\,dx$ and (c) northward transport $-\int_{x_W}^{x_E} \Phi_y(x,y)\,dx$ vs. y, for numerical solution in Fig. 2. For this solution, $W(x,y) = 0$ for $y_1 < y < y_2$, and $W(x,y) = 2.76$ for $y_S = 0 < y < y_1$.

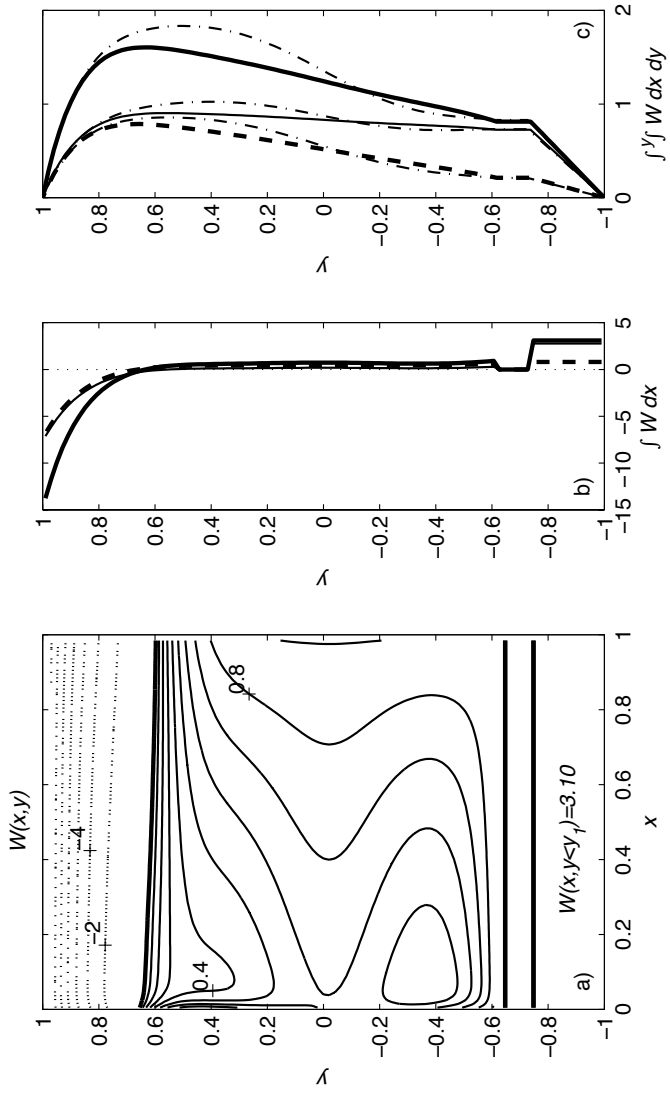

Figure 4: (a) Contours of W vs. x and y (CI = 1 for $W < 0$ and CI = 0.1 for $W > 0$)for numerical solution with $(\alpha_w, \alpha_e) = (4,1)$ and other parameters as in Fig. 2; for this solution, $W(x,y) = 3.10$ for $y_S < y < y_1$. Zonally integrated (b) vertical velocity $\int_{x_W}^{x_E} W(x,y)\,dx$ and (c) northward transport $-\int_{x_W}^{x_E} \Phi_y(x,y)\,dx$ vs. y, for numerical solutions with $(\alpha_w, \alpha_e) = \{(4,1),(2,1),(2,2)\}$ (thick solid line, thin solid, thick dashed, respectively)and other parameters as in Fig. 2. In (c), the corresponding analytical solutions for the zonally integrated northward transport are also shown (dash-dotted lines).

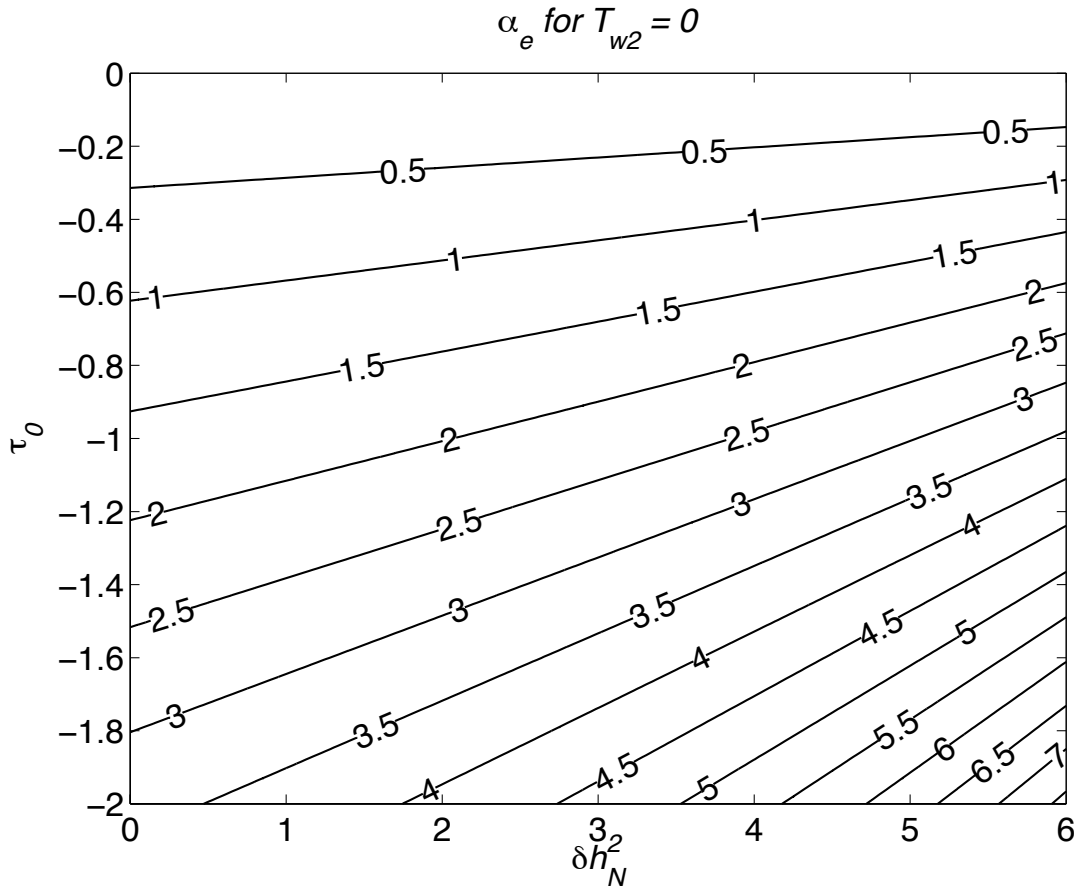

Figure 5: α_e vs. δh_N^2 and τ_0 for which the condition is met that $T_{w2} = 0$, from analytical solution and for other parameters as in Fig. 2.

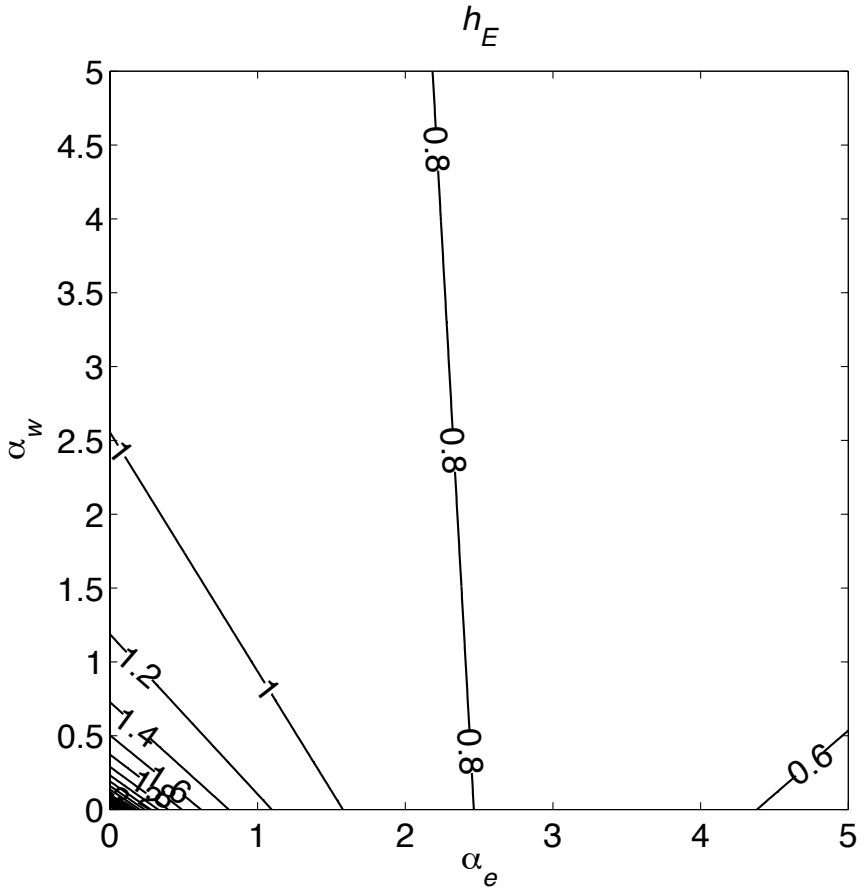

Figure 6: h_E vs. α_e and α_w, from analytical solution and for other parameters as in Fig. 2.

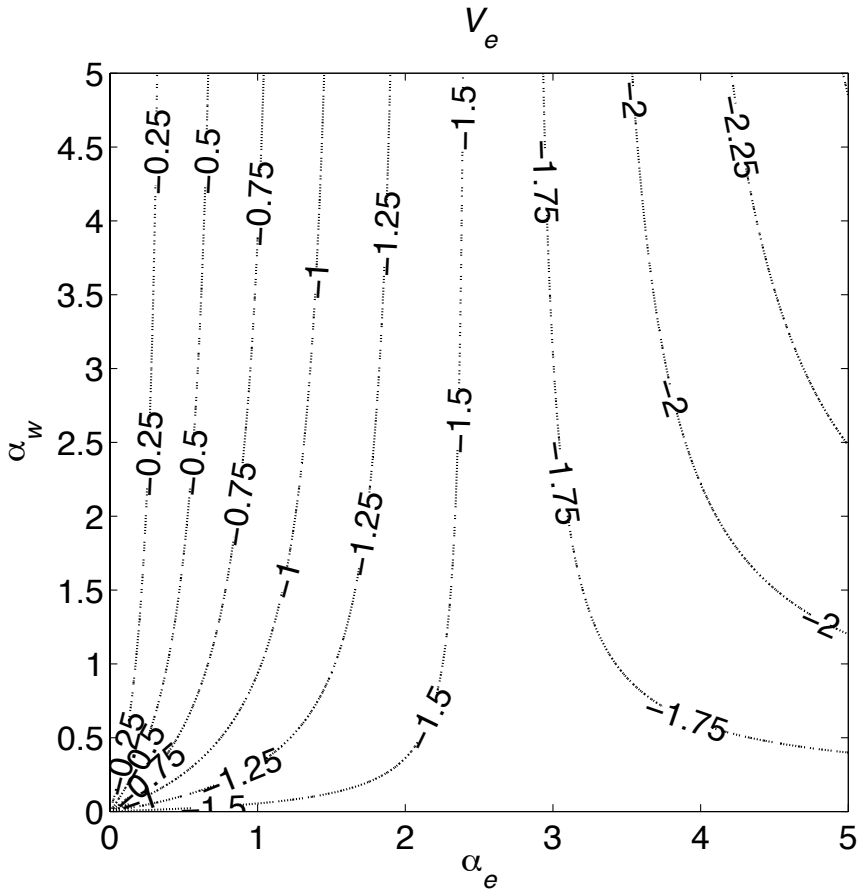

Figure 7: V_e vs. α_e and α_w, from analytical solution and for other parameters as in Fig. 2.

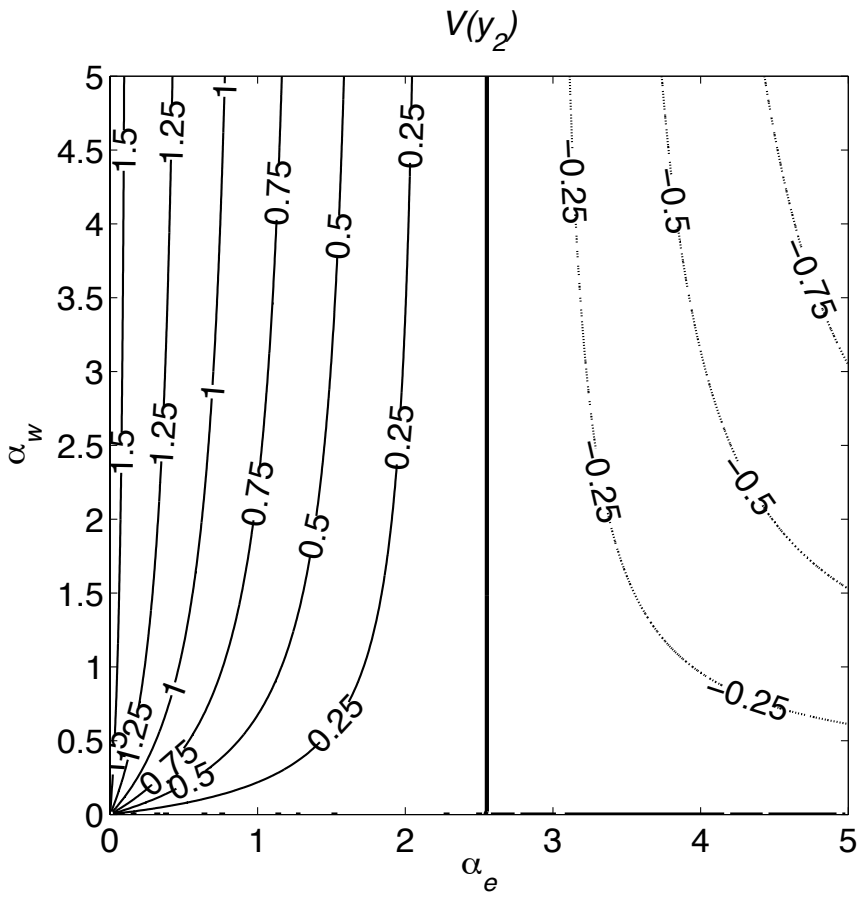

Figure 8: $V(y_2)$ vs. α_e and α_w, from analytical solution and for other parameters as in Fig. 2.

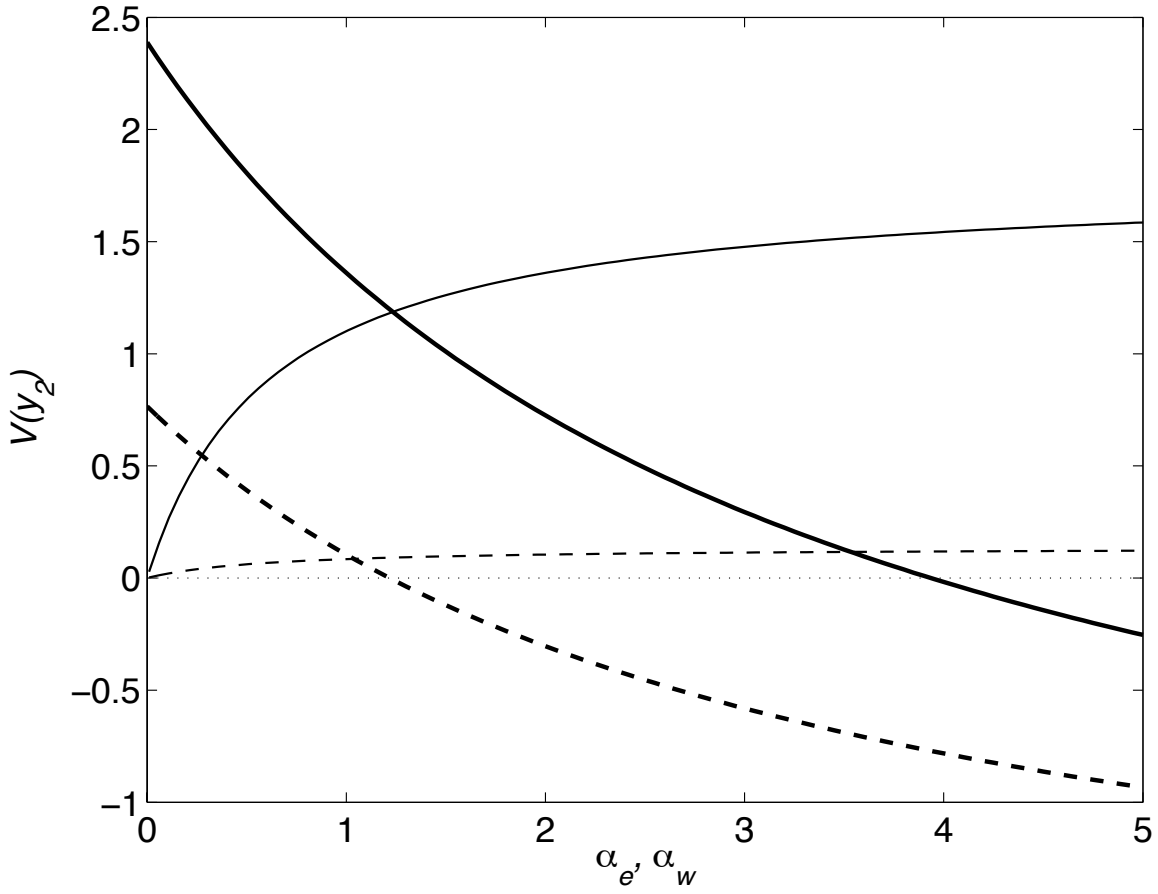

Figure 9: $V(y_2)$ vs. α_e (thick lines) and α_w (thin) for $\tau_1 = 0.5$ (solid) and $\tau_1 = -0.5$ (dashed), in each case from analytical solution and for other parameters as in Fig. 2. The corresponding dependencies on τ_1 for intermediate values of τ_1 are nearly linear.

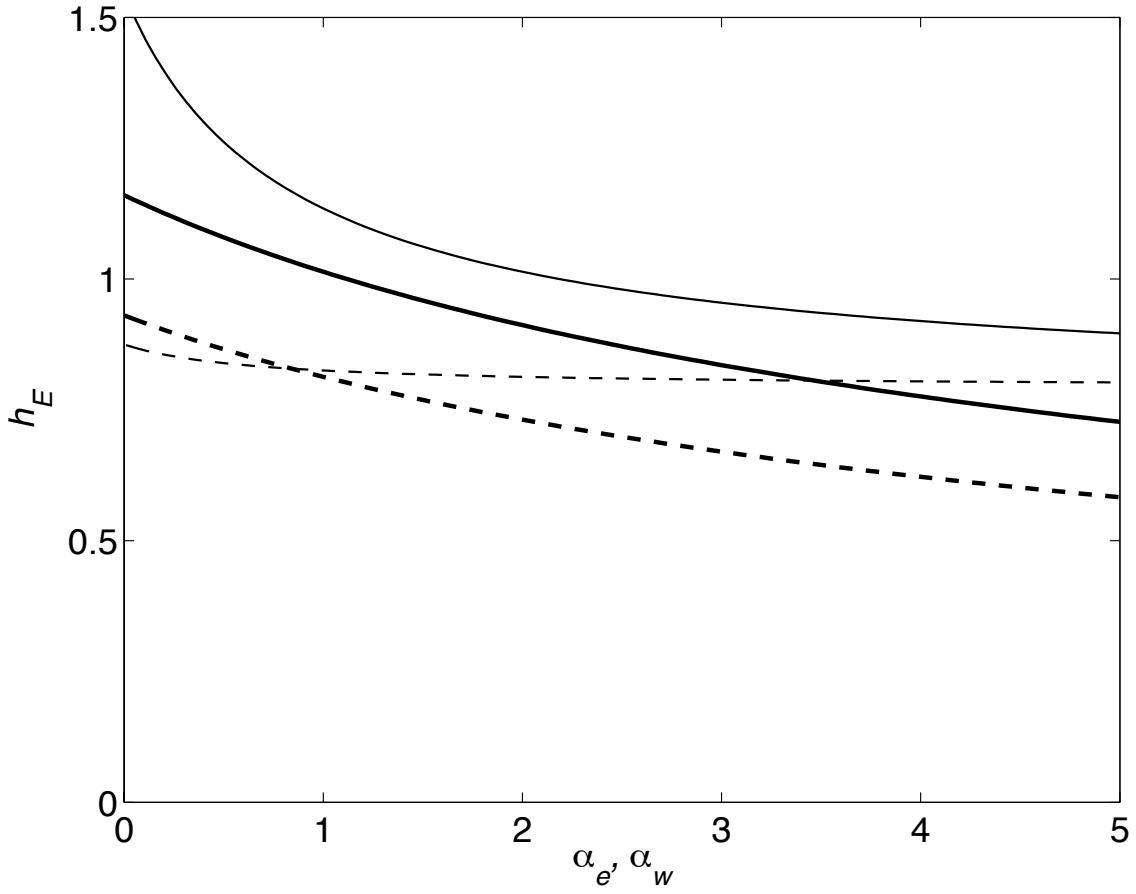

Figure 10: h_E vs. α_e (thick lines) and α_w (thin) for $\tau_1 = 0.5$ (solid) and $\tau_1 = -0.5$ (dashed), in each case from analytical solution and for other parameters as in Fig. 2. The corresponding dependencies on τ_1 for intermediate values of τ_1 are nearly linear.

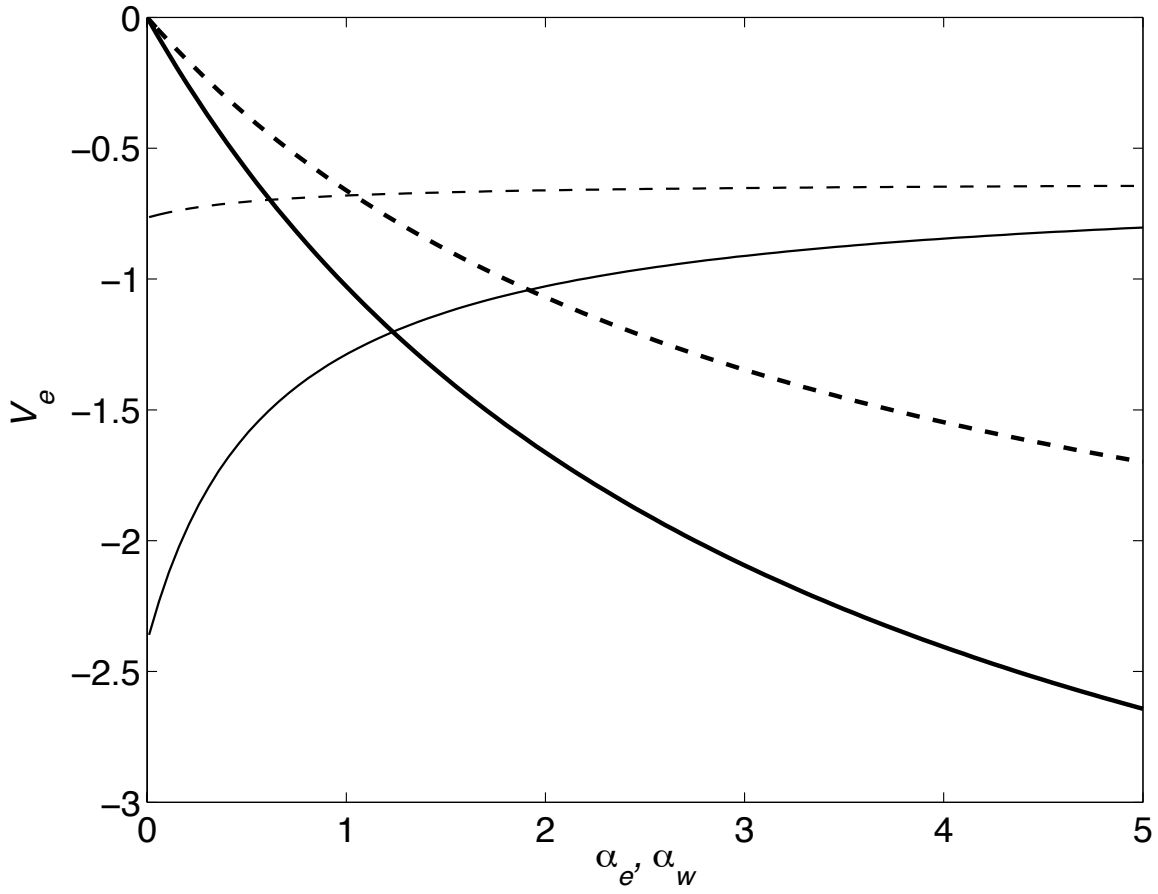

Figure 11: V_e vs. α_e (thick lines) and α_w (thin) for $\tau_1 = 0.5$ (solid) and $\tau_1 = -0.5$ (dashed), in each case from analytical solution and for other parameters as in Fig. 2. The corresponding dependencies on τ_1 for intermediate values of τ_1 are nearly linear.

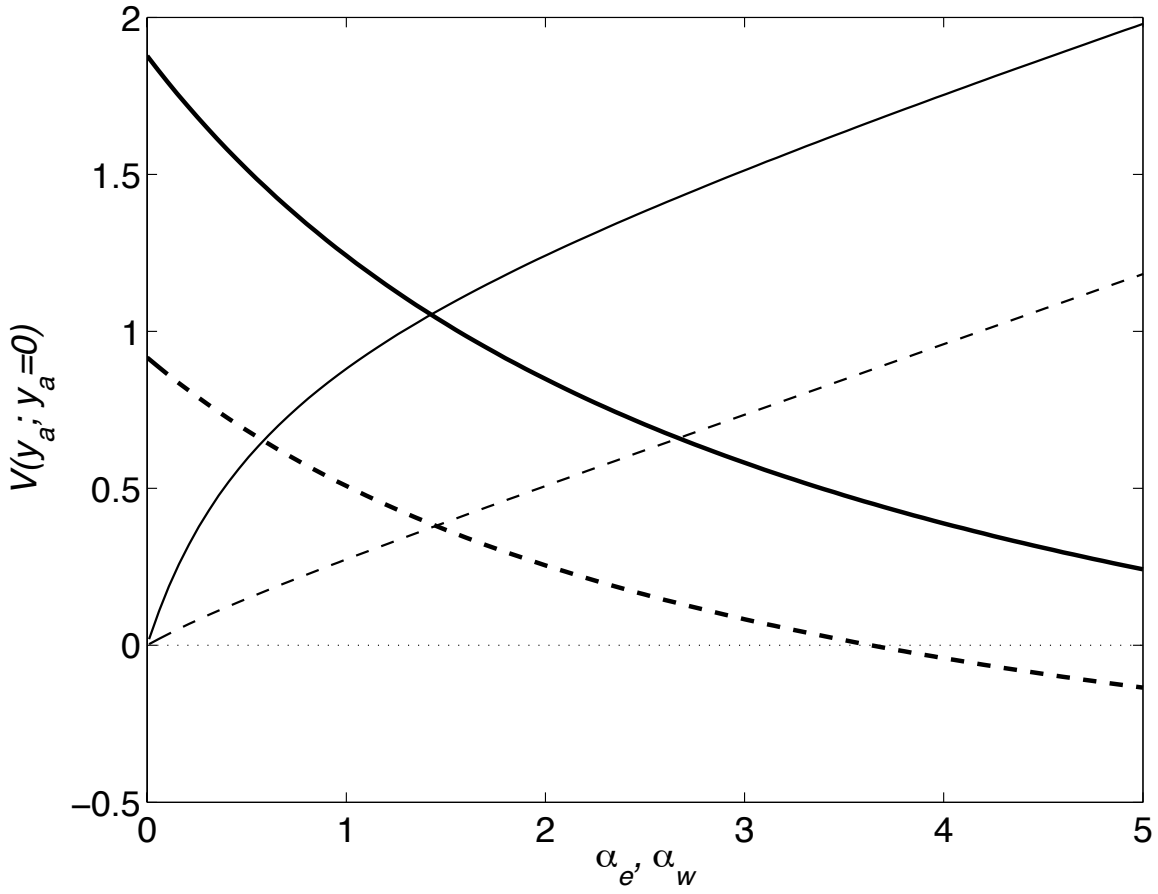

Figure 12: $V(y_a)$ for $y_a = 0$ vs. α_e (thick lines) and α_w (thin) for $\tau_1 = 0.5$ (solid) and $\tau_1 = -0.5$ (dashed), in each case from analytical solution and for other parameters as in Fig. 2. The corresponding dependencies on τ_1 for intermediate values of τ_1 are nearly linear.

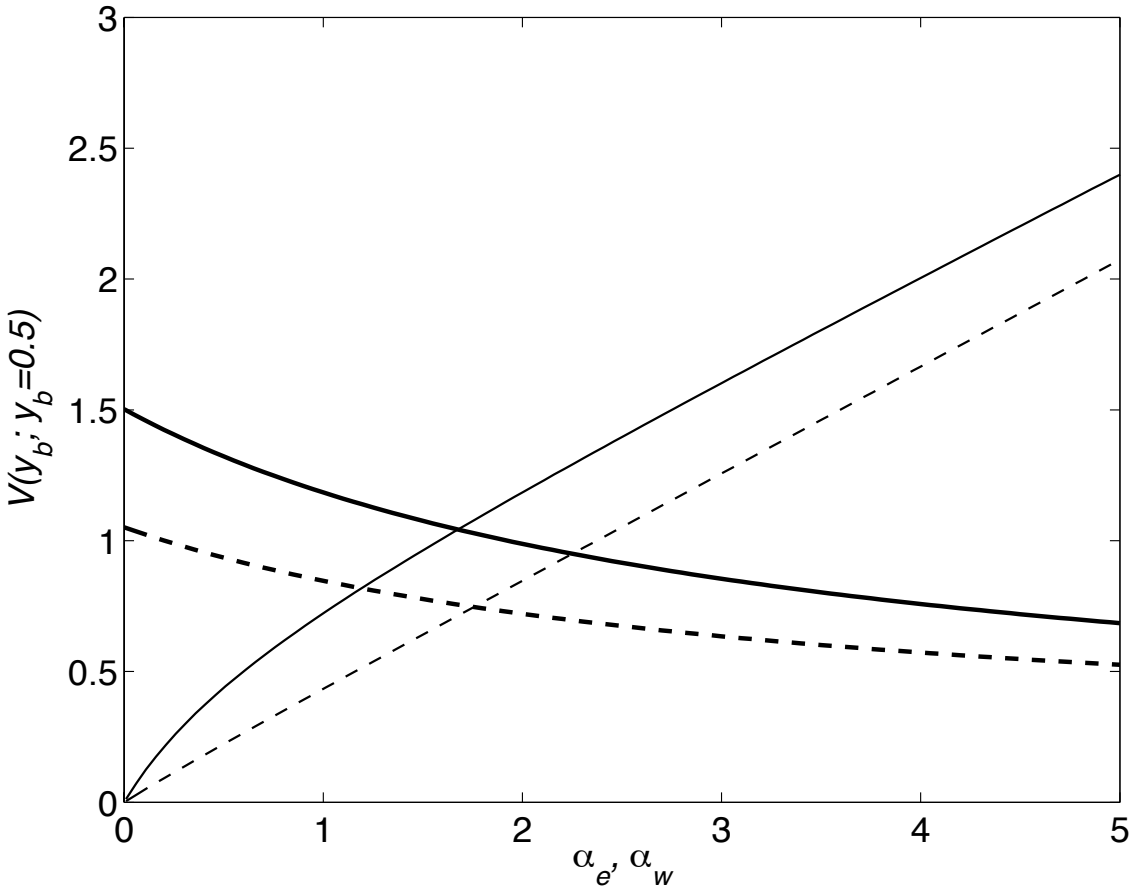

Figure 13: $V(y_b)$ for $y_b = 0.5$ vs. α_e (thick lines) and α_w (thin) for $\tau_1 = 0.5$ (solid) and $\tau_1 = -0.5$ (dashed), in each case from analytical solution and for other parameters as in Fig. 2. The corresponding dependencies on τ_1 for intermediate values of τ_1 are nearly linear.

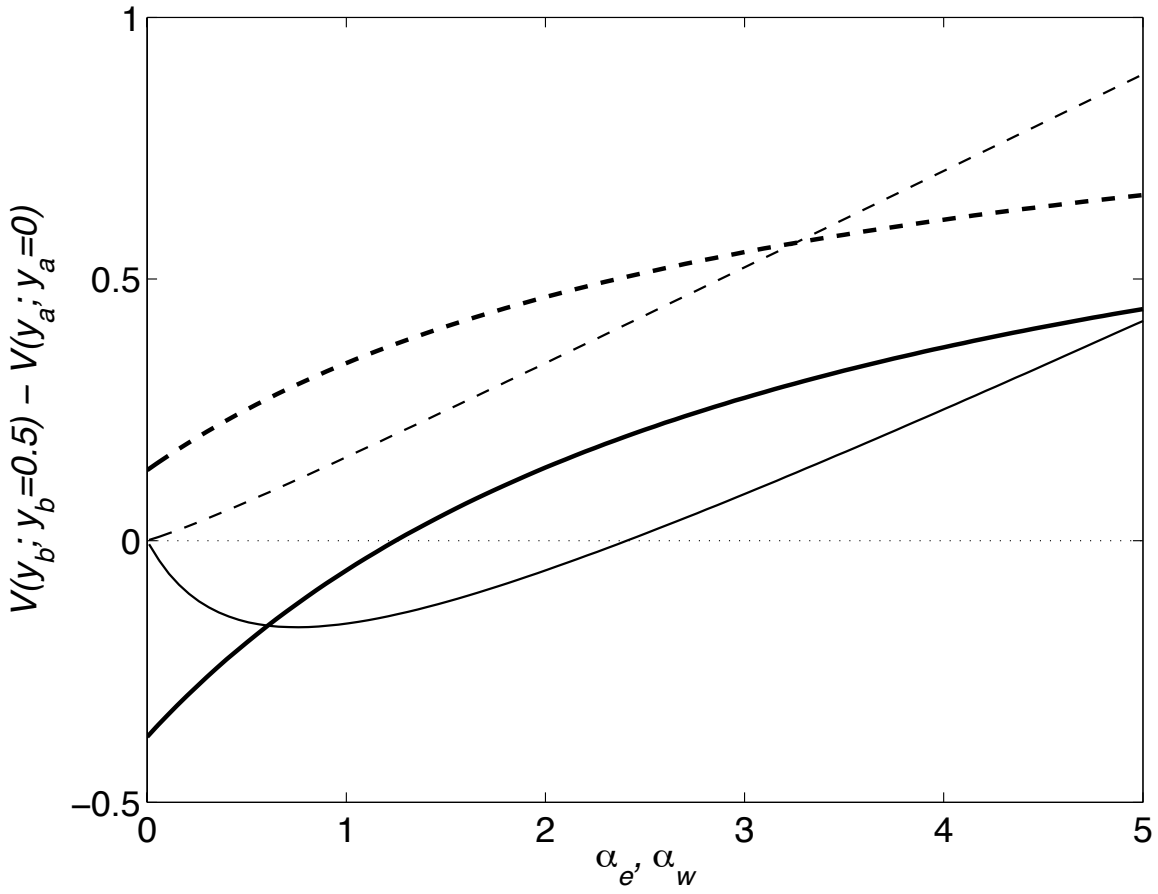

Figure 14: $V(y_b) - V(y_a)$ for $y_a = 0$ and $y_b = 0.5$ vs. α_e (thick lines) and α_w (thin) for $\tau_1 = 0.5$ (solid) and $\tau_1 = -0.5$ (dashed), in each case from analytical solution and for other parameters as in Fig. 2. The corresponding dependencies on τ_1 for intermediate values of τ_1 are nearly linear.